Desalination 320 (2013) 96–104

Contents lists available at SciVerse ScienceDirect

Desalination

journal homepage: www.elsevier.com/locate/desal

SMDDS design based on temporal flexibility analysis

Vincentius Surya Kurnia Adi, Chuei-Tin Chang *

Department of Chemical Engineering, National Cheng Kung University, Tainan, 70101, Taiwan, ROC

HIGHLIGHTS

- A systematic SMDDS design strategy is developed based on flexibility analysis.
- Appropriate design can be identified by computing the flexibility index of each candidate.
- An energy utilization ratio is introduced to facilitate proper decision making.
- The usefulness of temporal flexibility analysis is demonstrated with case studies.
- Both unit sizes and system structure can be properly determined.

ARTICLE INFO

Article history:
Received 7 February 2013
Received in revised form 11 April 2013
Accepted 12 April 2013
Available online xxxx

Keywords:
SMDDS design
AGMD module
Performance index
Temporal flexibility

ABSTRACT

A realistic *solar driven membrane distillation desalination system* (SMDDS) is expected to be fully functional in the presence of uncertain sunlight radiation and fluctuating freshwater demand. Since these time-variant disturbances and their cumulative effects can often be accommodated with a collection of properly-sized buffer units embedded in a suitable system configuration, a systematic SMDDS design strategy is thus developed in the present study on the basis of a novel quantitative measure. Specifically, a generic mathematical programming model is formulated for computing the temporal flexibility index of any given system. By assessing the operational flexibilities of alternative candidates, the most appropriate design can be identified accordingly. The results obtained in case studies show that the proposed approach is convenient and effective for addressing various operational issues in SMDDS design.

1. Introduction

Due to the alarming effects of global warming and a growing world population, there is an ever-increasing demand on water resources everywhere. In recent years, considerable effort has been devoted to the development of an efficient and sustainable desalination technology. Among all alternatives that utilize membrane distillation, the *air gap membrane distillation* (AGMD) is widely considered as a promising candidate since the energy consumed per unit of water generated by this method is the lowest [1–3]. Many researchers have already constructed rigorous mathematical models to simulate and analyze the underlying transport phenomena so as to identify the key variables affecting the water flux in an AGMD module [2,4–6]. In particular, Ben Bacha et al. [2] and Chang et al. [6,7] have built models of all units embedded in a *solar driven membrane distillation desalination system* (SMDDS), i.e., (1) the solar absorber, (2) the thermal storage tank, (3) the counter-flow shell-and-tube heat exchanger, (4) the AGMD modules, and (5) the distillate tank, and then discussed various operational and control issues accordingly. A typical process flow diagram of SMDDS can be found in Fig. 1. Gálvez et al. [8] meanwhile designed a 50 m^3/day desalination setup with an innovative solar-powered membrane, and Guillen-Burrieza et al. [9] also assembled a solar driven AGMD pilot. These two studies were performed with the common goal of minimizing energy consumption per unit of distillate produced. Although successful applications of the solar-driven AGMD modules were reported, it should be noted that the aforementioned works focused only upon thermal efficiency while the important issues concerning operational flexibility have never been addressed.

In fact, dealing with uncertainties is one of the practical issues that must be addressed in designing and operating any production process. A realistic SMDDS design is expected to be fully functional in the presence of uncertain sunlight radiation and fluctuating freshwater demand. Traditionally, the ability of a system to maintain feasible operation despite unexpected disturbances is referred to as its *operational flexibility*. Various approaches have been proposed to determine a quantitative performance measure so as to facilitate flexibility analysis [10–26]. The original *flexibility index* (FI_s) was first defined by Swaney and Grossmann [14,15] which is to be used as an unambiguous gauge of the feasible region in the uncertain parameter space. Specifically, the value of FI_s is associated with the maximum allowable deviations of the uncertain parameters from their nominal values, by which feasible operation can be assured with proper manipulation of the control

* Corresponding author. Tel.: +886 6 275 7575x62663; fax: +886 6 234 4496.
E-mail address: ctchang@mail.ncku.edu.tw (C.-T. Chang).

0011-9164/$ – see front matter © 2013 Elsevier B.V. All rights reserved.
http://dx.doi.org/10.1016/j.desal.2013.04.009

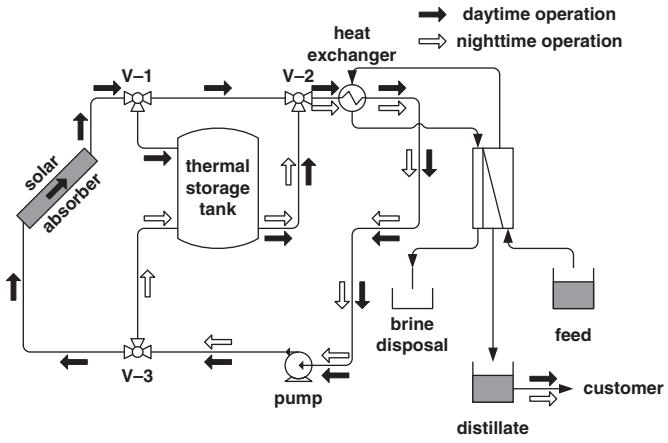

Fig. 1. Configuration I.

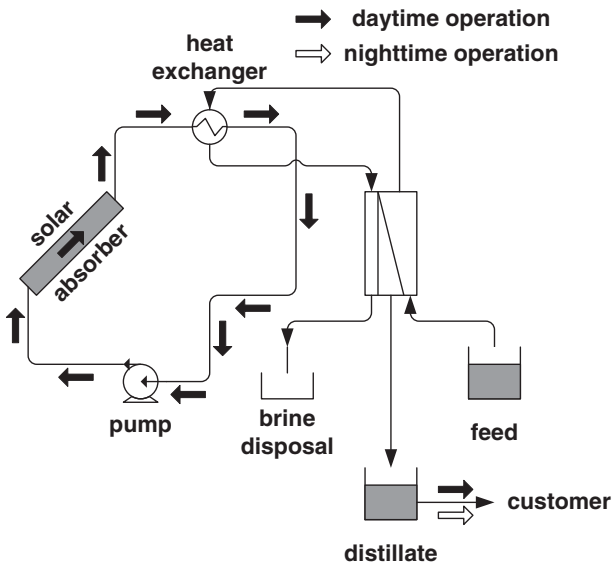

Fig. 2. Configuration II.

variables. These authors also showed that, under certain convexity assumptions, critical points that limit feasibility and/or flexibility must lie on the vertices of the uncertain parameter space [15]. Grossmann and Floudas [18] later exploited the fact that the active constraints are responsible for limiting the flexibility of a design and developed a mixed integer nonlinear programming (MINLP) model accordingly. Similar flexibility analysis was also carried out in a series of subsequent studies to produce resilient grassroots and revamp designs [27,28]. Since the steady-state material-and-energy balances are used as the equality constraints in the aforementioned MINLP models [14,15,18,19,21,23,25], the traditional steady-state flexibility index should be regarded as a performance indicator of the *continuous* processes [29–33]. On the other hand, as indicated by Dimitriadis and Pistikopoulos [34], the operational flexibility of a *dynamic* system should be evaluated differently. By adopting a system of differential algebraic equations (DAEs) as the model constraints, they developed a mathematical programming formulation for computing the dynamic flexibility index (FI_d). Clearly this practice is more rigorous than that based on the steady-state model since, even for a continuous process, the operational flexibility cannot be adequately characterized without accounting for the transient dynamics.

In the aforementioned dynamic flexibility analysis, the nominal values of uncertain parameters and the anticipated positive and negative deviations in these parameters were assumed to be available at every instance over the entire time horizon of operation life. The corresponding flexibility index can be uniquely determined on the basis of a dynamic system model and also such a priori information. However, while the unexpected fluctuations in some process parameters may render an ill-designed system inoperable at certain instances, their cumulative effects can also result in serious consequences. The latter scenario is completely ignored in the traditional dynamic flexibility analysis, but it is in fact a more probable event in SMDDS operations. This is because, in the former case, the immediate impacts of instantaneous disturbances in solar irradiation and freshwater demand can usually be absorbed by the thermal storage tank and/or the distillate tank. In a previous study, Adi and Chang [35] developed a generic mathematical program to compute *temporal flexibility index* (FI_t) for quantifying the system's ability to buffer the accumulated changes in process parameters. This index should be regarded as a useful criterion for identifying realistic SMDDS designs. Specifically, all units in Configuration I (see Fig. 1) can be properly sized to achieve a target FI_t. Notice that various structural issues can also be addressed. For example, several alternative thermal storage schemes can be evaluated on the basis of temporal flexibility analysis. The stripped-down version of SMDDS design in Fig. 2 (Configuration II) can certainly be analyzed and compared with Configuration I, while installation of an extra thermal storage tank (say, on an additional bypass from solar absorber to heat exchanger and/or vice versa) can also be considered.

The rest of the paper is organized as follows. The mathematical models of SMDDS units are first presented in the next section. Next, in Section 3, the novel concept of temporal flexibility is outlined and a generic programming formulation (for computing FI_t) is also given. A series of extensive case studies have been performed to validate the proposed design approach in this work. The optimization and simulation results on the two configurations in Figs. 1 and 2 are thoroughly analyzed and discussed in Section 4. Finally, conclusions are drawn in Section 5.

2. Mathematical models of SMDDS units

The aforementioned SMDDS units, i.e., the solar absorber, the thermal storage tank, the counter-flow shell-and-tube heat exchanger, the AGMD modules, and the distillate tank, are interconnected in a typical system to form two separate processing routes for seawater desalination and solar energy conversion respectively. For implementation convenience, the available unit models [6] have been simplified and these modified versions are outlined below.

- Solar absorber

The solar absorber in a SMDDS design is used to convert solar energy to heat. The following assumptions are adopted in formulating its mathematical model: (1) the fluid velocities in all absorber tubes are the same; (2) the fluid temperature should be kept below boiling point; (3) there is no water loss; and (4) heat loss is negligible. The corresponding transient energy balance can be written as

$$\frac{dT_{f,SA_{out}}}{dt} = -L_{SA}\frac{m_{f,SA}}{M_{f,SA}}\frac{T_{f,SA_{out}} - T_{f,SA_{in}}}{L_{SA}} + \frac{A_{SA}I(t)}{M_{f,SA}Cp_f^L} \tag{1}$$

$$T_{f,SA_{out}} \le T_{f,SA_{out}}^{max} \tag{2}$$

where, $T_{f,SA_{in}}$ and $T_{f,SA_{out}}$ denote the inlet and outlet temperatures (°C) of the solar absorber respectively; $T_{f,SA_{out}}^{max}$ is the maximum allowable outlet temperature (°C); $M_{f,SA}$ denotes the total mass of operating fluid in the solar absorber (kg); $m_{f,SA}$ denotes the overall mass flow rate of operating fluid in solar absorber (kg/h); L_{SA} is the length of an absorber tube (m); A_{SA} is the exposed area of a solar absorber (m^2); Cp_f^L is the heat

capacity of operating fluid (J/kg °C); and $I(t)$ is the solar irradiation rate per unit area (W/m^2).

• Thermal storage tank

By assuming that (1) the fluid inside the thermal storage tank is well mixed, (2) the inlet and outlet flow rates are identical, and (3) the heat capacity of operating fluid is independent of temperature, the energy balance around thermal storage tank can be expressed as

$$M_{f,ST}\frac{dT_{f,ST_{out}}}{dt} = r_{f,ST}m_{f,STL}\left(T_{f,ST_{in}} - T_{f,ST_{out}}\right) \tag{3}$$

$$r_{f,ST} = \frac{m_{f,ST}}{m_{f,STL}} \tag{4}$$

where, $T_{f,ST_{in}}$ and $T_{f,ST_{out}}$ denote the inlet and outlet temperatures (°C) respectively; $M_{f,ST}$ represents the total mass of operating fluid in the thermal storage tank (kg); $m_{f,STL}$ is the total mass flow rate driven by the pump in the thermal loop (kg/h); and $m_{f,ST}$ is the throughput of thermal storage tank (kg/h) which equals $r_{f,ST}m_{f,STL}$.

In Configuration I, the solar absorber is connected to the thermal loop only during daytime operation. In other words,

$$m_{f,SA} = \begin{cases} m_{f,STL} & \text{if } I(t) > 0 \text{ (daytime)} \\ 0 & \text{if } I(t) = 0 \text{ (nighttime)} \end{cases}. \tag{5}$$

As a result, the flow ratio defined in Eq. (4) can be treated as an adjustable control variable in daytime operation, i.e., $0 \le r_{f,ST}(t) \le 1$, while $r_{f,ST}(=1)$ is kept unchanged during nighttime.

Finally, in the case if the thermal storage tank is not utilized, i.e., Configuration II, there is really no need to distinguish the operation modes and thus one can simply fix $m_{f,SA} = m_{f,STL}$ and $r_{f,ST} = 0$.

• Heat exchanger

The hot fluid used in the counter-flow heat exchanger comes from the thermal storage tank and/or solar absorber, while the cold fluid is the sea water. The dynamics in this unit are ignored and a steady-state energy balance is used to model the heat-exchange process. It is also assumed that there is no heat loss. Thus, the unit model of heat exchanger can be written as

$$m_{f,MD}\left(T_{f,HX,CL_{out}} - T_{f,HX,CL_{in}}\right) = m_{f,HX,HL}\left(T_{f,HX,HL_{in}} - T_{f,HX,HL_{out}}\right) \tag{6}$$

where, $m_{f,HX,HL}$ is the mass flow rate of hot fluid (kg/h); $T_{f,HX,HL_{in}}$ and $T_{f,HX,HL_{out}}$ respectively denote the inlet and outlet temperatures of hot fluid (°C); $m_{f,MD}$ is the mass flow rate of sea water in membrane distillation loop (kg/h); and $T_{f,HX,CL_{in}}$ and $T_{f,HX,CL_{out}}$ respectively denote the inlet and outlet temperatures of the cold fluid (°C). Note that the mass flow rate of hot fluid is essentially the same as that in the thermal loops in both Configurations I and II, i.e.

$$m_{f,HX,HL} = m_{f,STL}. \tag{7}$$

An energy balance around the valve V-2 yields

$$T_{f,HX,HL_{in}} = \left(1 - r_{f,ST}\right)T_{f,SA_{out}} + r_{f,ST}T_{f,ST_{out}}. \tag{8}$$

Again, this equation is also valid in the above two structures. Finally, let us consider the outlet temperature of hot fluid. Since, in Configuration I, the hot fluid leaving heat exchanger is recycled back to the solar absorber in the daytime operation and to the thermal storage tank during nighttime, the following constraints should be imposed

$$T_{f,HX,HL_{out}} = \begin{cases} T_{f,SA_{in}} & \text{if } I(t) > 0 \text{ (daytime)} \\ T_{f,ST_{in}} & \text{if } I(t) = 0 \text{ (nighttime)} \end{cases}. \tag{9}$$

On the other hand, since Configuration II is not equipped with a thermal storage tank, only the first constraint in Eq. (9) can be used in the corresponding model.

• AGMD module

To enhance computation efficiency, only a simplified model is adopted in this study for charactering the AGMD unit. It is assumed that the mass flux of distillate across membrane is a function of the rate of energy input. Specifically, this flux in a standard module can be expressed as

$$N_{mem} = \frac{m_{f,MD}Cp_f^L\left(T_{f,HX,CL_{out}} - T_{f,HX,CL_{in}}\right)}{STEC \cdot A_{MD} \cdot n_{AGMD}} \tag{10}$$

where, N_{mem} denotes the distillate flux (kg/m^2 h); A_{MD} is the fixed membrane area of a standard AGMD module (m^2); n_{AGMD} is the total number of standard modules; and STEC is the *specific thermal energy consumption* constant (kJ/kg), which can be considered as the ratio between energy supplied by the heat exchanger and mass of the distillate produced [36,37].

Strictly speaking, the mass flux through AGMD membrane should be driven primarily by the vapor pressure differential. However, this flux is assumed here to be roughly proportional to the temperature difference for the purpose of simplifying calculation. Since Eq. (10) is used essentially as an empirical relation in this case, it should be only valid within a finite range of the sea water flow rate. Consequently, $m_{f,MD}$ is treated in this work as an adjustable control variable which is allowed to vary $\pm 10\%$ from its nominal value.

$$0.9m_{f,MD}^N \le m_{f,MD} \le 1.1m_{f,MD}^N \tag{11}$$

Finally, note that the sea water entering AGMD module should not be allowed to exceed a specified upper bound so as to avoid damaging the membrane, i.e.

$$T_{f,HX,CL_{out}} \le T_{f,HX,CL_{out}}^{max} \tag{12}$$

where, $T_{f,HX,CL_{out}}^{max}$ is the upper bound of a cold stream temperature at the outlet of a heat exchanger (°C).

• Distillate tank

The distillate tank is used as the buffer for the fluctuating water demand. The corresponding model can be written as

$$\rho_f^L A_{DT}\frac{dh_{DT}}{dt} = m_{f,DT_{in}} - m_{f,DT_{out}} \tag{13}$$

where, ρ_f^L is the distillate density (kg/m^3); A_{DT} is the cross-sectional area of distillate tank (m^2); h_{DT} is the height of liquid in distillate tank (m); $m_{f,DT_{in}}$ and $m_{f,DT_{out}}$ denote the inlet and outlet flow rates respectively (kg/h). Note that the inlet flow is produced by the AGMD unit, i.e.

$$m_{f,DT_{in}} = n_{AGMD}N_{mem}A_{MD}. \tag{14}$$

Finally, it is obvious that the liquid height in the distillate tank should be maintained within a specified range, i.e.

$$h_{DT,low} \le h_{DT} \le h_{DT,high} \tag{15}$$

where, $h_{DT,low}$ and $h_{DT,high}$ respectively denote the given lower and upper bounds (m).

3. Temporal flexibility analysis

To facilitate clear explanation of the novel concept of temporal flexibility, let us briefly review the conventional formulations for steady-state flexibility analysis [14,15]. For illustration convenience, the following label sets should be first defined:

$$\mathbb{I} = \{i | i \text{ is the label of an equality constraint}\} \tag{16}$$

$$\mathbb{J} = \{j | j \text{ is the label of an inequality constraint}\}. \tag{17}$$

The general design model of a steady-state system can be expressed accordingly as

$$f_i(\mathbf{d}, \mathbf{z}, \mathbf{x}, \boldsymbol{\theta}) = 0, \quad \forall i \in \mathbb{I} \tag{18}$$

$$g_j(\mathbf{d}, \mathbf{z}, \mathbf{x}, \boldsymbol{\theta}) \le 0, \quad \forall j \in \mathbb{J} \tag{19}$$

where, f_i is the i^{th} equality constraint in the design model (e.g., the mass or energy balance equation for a processing unit); g_j is the j^{th} inequality constraint (e.g., a capacity limit); $\mathbf{d}$ represents a vector which contains the design variables corresponding to the structure and equipment sizes of the plant; $\mathbf{z}$ denotes a vector which contains the control variables that can be adjusted during operation, e.g., flows and utility loads; $\mathbf{x}$ is a vector which contains the state variables that define the system, e.g., concentrations, temperatures and pressures; $\boldsymbol{\theta}$ denotes the vector which contains the uncertain parameters, e.g., inlet conditions and reaction rate constants [38].

Given a nominal parameter value $\boldsymbol{\theta}^N$ and the corresponding expected deviations in the positive and negative directions ($\Delta\boldsymbol{\theta}^+$ and $\Delta\boldsymbol{\theta}^-$), the uncertain parameters can be constrained accordingly as

$$\boldsymbol{\theta}^N - \delta\Delta\boldsymbol{\theta}^- \le \boldsymbol{\theta} \le \boldsymbol{\theta}^N + \delta\Delta\boldsymbol{\theta}^+ \tag{20}$$

where, δ is a positive scalar variable to be determined with the flexibility analysis. In the original formulation, the flexibility index represents the largest deviation that the design can accommodate while remaining feasible, i.e., satisfying Eqs. (18) and (19). For a fixed design with constant $\mathbf{d}$, this *steady-state flexibility index* can be determined by solving the following model:

$$FI_s = \max \delta \tag{21}$$

subject to the constraints in Eqs. (18), (20) and those presented below

$$\max_{\boldsymbol{\theta}} \min_{\mathbf{z}} \max_{j} g_j(\mathbf{d}, \mathbf{z}, \mathbf{x}, \boldsymbol{\theta}) \le 0. \tag{22}$$

It should be noted that $FI_s \ge 1$ indicates that the flexibility target is reached for the corresponding steady-state operations.

Dimitriadis and Pistikopoulos [34] replaced the equality constraints in Eq. (18) with a system of differential-algebraic equations, i.e.

$$f_i(\mathbf{d}, \mathbf{z}(t), \mathbf{x}(t), \dot{\mathbf{x}}(t), \boldsymbol{\theta}(t)) = 0 \tag{23}$$

where, $t \in [0, H]$, $i \in \mathbb{I}$, and $\mathbf{x}(0) = \mathbf{x}^0$. Thus, the *dynamic flexibility index* can be computed with the following model:

$$FI_d = \max \delta \tag{24}$$

subject to Eq. (23) and

$$\max_{\boldsymbol{\theta}(t)} \min_{\mathbf{z}(t)} \max_{j,t} g_j(\mathbf{d}, \mathbf{z}(t), \mathbf{x}(t), \boldsymbol{\theta}(t), t) \le 0 \tag{25}$$

$$\boldsymbol{\theta}^N(t) - \delta\Delta\boldsymbol{\theta}^-(t) \le \boldsymbol{\theta}(t) \le \boldsymbol{\theta}^N(t) + \delta\Delta\boldsymbol{\theta}^+(t). \tag{26}$$

Note that time is introduced in this model as an independent variable since it is necessary to characterize the system dynamics. Notice also that the scope of dynamic flexibility analysis must cover the *entire* operation horizon $[0,H]$ and the variations in the parameters $\boldsymbol{\theta}(t)$ are bounded at every instance according to Eq. (26). These requirements on uncertain parameters may be too restrictive for practical applications, since a system can be still feasible even under the condition that the "short-term" disturbances exceed the given limits temporarily.

To facilitate the temporal flexibility analysis, let us assume that the variations in uncertain parameters are possible within a finite time interval $[t_0,t_1] \subset [0,H]$. The cumulative effects of short-term disturbances can be assessed by integrating Eq. (26), i.e.

$$-\delta\int_{t_0}^{t_1}\Delta\boldsymbol{\theta}(\tau)^- d\tau \le \int_{t_0}^{t_1}\left(\boldsymbol{\theta}(\tau) - \boldsymbol{\theta}(\tau)^N\right)d\tau \le \delta\int_{t_0}^{t_1}\Delta\boldsymbol{\theta}(\tau)^+ d\tau. \tag{27}$$

Since the anticipated largest possible deviations in uncertain parameters should be regarded as given information, the expected *net* positive and negative cumulated deviations over interval $[t_0,t_1]$, i.e., $\int_{t_0}^{t_1}\Delta\boldsymbol{\theta}(\tau)^- d\tau$ and $\int_{t_0}^{t_1}\Delta\boldsymbol{\theta}(\tau)^+ d\tau$, can also be computed in advance. To ensure operational safety, these net upper and lower bounds are adopted in this work to limit the accumulated effects at any time. For clarity, let us simplify notation as follows:

$$\begin{aligned} \Delta\Theta^- &= \int_{t_0}^{t_1}\Delta\boldsymbol{\theta}(\tau)^- d\tau \\ \Delta\Theta^+ &= \int_{t_0}^{t_1}\Delta\boldsymbol{\theta}(\tau)^+ d\tau \end{aligned} \tag{28}$$

$$\Theta(t) = \int_{t_0}^{t}\left(\boldsymbol{\theta}(\tau) - \boldsymbol{\theta}(\tau)^N\right)d\tau \tag{29}$$

Eq. (27) can be modified accordingly as

$$-\delta\Delta\Theta^- \le \Theta(t) \le \delta\Delta\Theta^+. \tag{30}$$

Furthermore, since the time interval $[t_0,t_1]$ itself may also be uncertain, Eq. (29) can be rewritten as:

$$\frac{d}{dt}\Theta(t) = \boldsymbol{\theta}(t) - \boldsymbol{\theta}^N(t) \tag{31}$$

where, $\Theta(0) = \mathbf{0}$ and $t \in [0,H]$. Eqs. (23), (25), (28), (30) and (31) can then be used as the constraints of a mathematical programming model to determine the temporal flexibility index FI_t by maximizing the scalar variable δ [35]. The required calculation procedure is presented schematically in Fig. 3.

4. Case studies

The case studies presented below are used mainly to demonstrate the important role of temporal flexibility index in SMDDS design. In all examples considered in this section, the specifications of a standard AGMD module are assumed to be the same as those given in Banat et al. [36]. In particular, every module is equipped with a hydrophobic porous membrane, a hot and a cold water flow channel, and an air layer between the membrane and the cold seawater channel. The membrane is made of polytetrafluoroethylene (PTFE) having an effective area of 10 m^2 per module. The flow channels are fabricated by spiral winding the membrane and condenser foils. The effluent of cold seawater flows into the shell side of a heat exchanger and then into the hot flow channel of an AGMD unit. Because of the hydrophobic nature of porous membrane, only water vapor can be transferred through the membrane pore and this flux is driven primarily by the partial pressure difference across the membrane [36]. The transported water vapor is condensed on the wall surface of cold seawater flow channel and then collected in a distillate tank for domestic consumption.

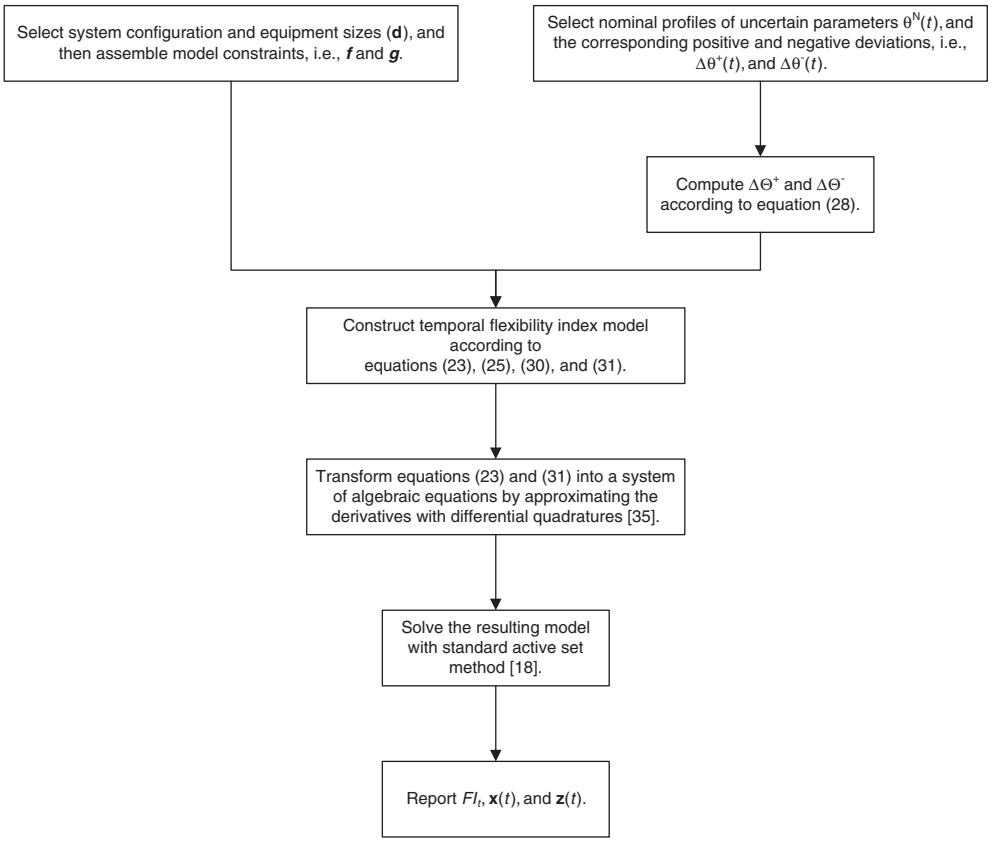

Fig. 3. Computation procedure for a temporal flexibility index.

From Figs. 1 and 2, it can be clearly observed that the AGMD desalination unit is driven by the thermal energy carried in the operating fluid (which is water in the present case studies). In the daytime operation, the heat generated by the solar absorber can be consumed entirely in either Configuration I or II if the irradiation level is low. In the case of strong sunlight, a portion of the absorbed energy can be kept in the thermal storage tank of Configuration I and then used later to enable an extended period of desalination operation after sunset. Since Configuration II is not equipped with any thermal storage facility, it is therefore necessary to utilize a relatively small absorber so as to ensure complete consumption of solar energy in daytime operation and satisfy the freshwater demand during the night with a large enough distillate tank.

The solar irradiation rate $I(t)$ is regarded as a time-variant uncertain parameter in the temporal flexibility analysis. Its nominal profile $I^N(t)$, which is similar to that suggested by Chang et al. [7], and the expected upper and lower bounds are all depicted in Fig. 4. Note that the expected positive and negative deviations at any time are both set at 10% of the nominal level. The water demand rate $m_{f,DT_{out}}(t)$ is another uncertain parameter considered in the case studies. Its nominal value is set at 18 kg/h × $wdf(t)$, where $wdf(t)$ is the ratio between the demand rate at time t and a reference value, i.e., 18 kg/h. The expected deviations in $m_{f,DT_{out}}$ are also selected to be 10% of its nominal value. The nominal level of $wdf(t)$ and also the corresponding upper and lower limits are sketched in Fig. 5. It is assumed that the time-dependent household water consumption rate can be closely characterized by the nominal profile of $wdf(t)$. Finally, it should be noted that, if more realistic solar irradiation profile and water demand profile are available in the future, they can be easily incorporated in the proposed flexibility analysis so as to acquire better designs.

Before solving the proposed mathematical programs, all model parameters must be properly selected. Based on Eqs. (10) and (14), the production rate of each AGMD module at $T_{f,HX,CL_{out}} = 74$ °C is estimated to be 16.54 kg/h [36] (assuming that the feed temperature is $T_{f,HX,CL_{in}} = 25$ °C). The nominal mass flow rate of sea water in membrane distillation loop $m^N_{f,MD}$ is set to be 1125 kg/h per AGMD module according to Banat et al. [36]. Also, a maximum daily demand of 750.42 kg/day can be computed according to Fig. 5. By adopting an average online period of 12 h/day, the approximate number of parallel AGMD modules can be calculated: $n_{AGMD} = \frac{750.42}{16.54 \times 12} = 3.78 \approx 4$, thus the total membrane area is 40 m^2. In the solar absorber, the total mass of operating fluid per unit area, i.e., $M_{f,SA}/A_{SA}$, is set to be 15 kg/m^2 [6]. The flow rate in solar thermal loop ($m_{f,STL}$) is chosen to be 36,000 kg/h, which is 8 times the total nominal flow rate of sea water in the membrane distillation loop ($m^N_{f,MD} = 1125 \times 4 = 4500$ kg/h). This value is selected to ensure quick temperature response in the desalination loop. The volume of distillate tank in

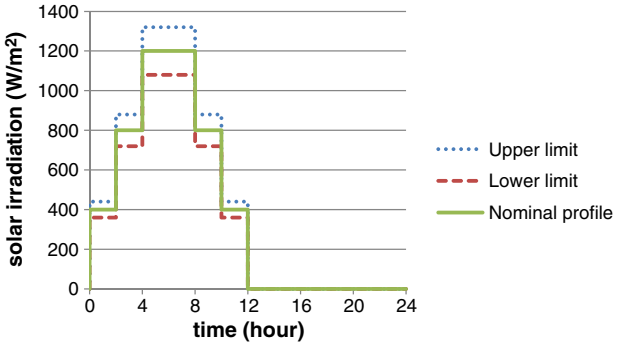

Fig. 4. Solar irradiation profile.

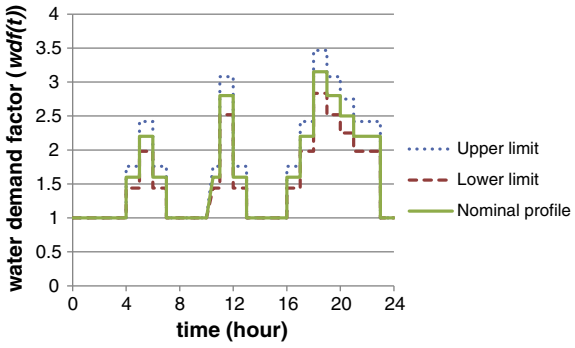

Fig. 5. Normalized water demand profile.

each configuration is assumed to be 0.75 m^3 ($A_{DT} = 0.35\ m^2$; $h_{DT,low} = 0$ m; $h_{DT,high} = 2.14$ m), while a 10 m^3 thermal storage tank ($M_{f,ST} = 10{,}000$ kg) is utilized in Configuration I. Finally, it is assumed that the heat capacity of operating fluid Cp_f^L is held constant at 4200 J/kg °C and its density ρ_f^L is also assumed to be constant at 1000 kg/m^3.

As mentioned previously, the solar absorber should be sized according to the AGMD capacity. To facilitate proper decision, the asymptotic energy utilization ratio between these two units should be first considered:

$$\phi_{util} = \frac{\text{maximum supply rate of solar energy}}{\text{maximum consumption rate of thermal energy}} = \frac{A_{SA} I(t)^{max}}{m_{f,MD}^{max} Cp_f^L \left(T_{f,HX,CL_{out}}^{max} - T_{f,HX,CL_{in}}^{min}\right)}. \quad (32)$$

Obviously, the energy collected by the solar absorber can be fully utilized by the AGMD module if $\phi_{util} \le 1$. Otherwise, there should be a need to store the excess heat. From Fig. 4, it can be observed that $I(t)^{max} = 1320\ W/m^2$. On the basis of Eq. (11), one could deduce $m_{f,MD}^{max} = 1.1 m_{f,MD}^{N} = 1237.5$ kg/h. Also, from the model description given in Section 2, it is reasonable to assume that $T_{f,HX,CL_{out}}^{max} = 90$ °C and $T_{f,HX,CL_{in}}^{min} = 25$ °C. Note that only a simple calculation is needed for sizing the solar absorber according to a given ϕ_{util} For example, the absorber area for $\phi_{util} = 1$ should be $A_{SA} = \frac{1237.5 \times 4200 \times (90-25)}{1320 \times 3600} = 71.09\ m^2$. For the sake of completeness, all model parameters and variables used in the case studies are also listed in Table 1.

A systematic approach is followed in this work to size the solar absorber on the basis of Eq. (32) and a given AGMD module size. By adopting the aforementioned thermal storage tank and a distillate tank, the temporal flexibility indices of Configurations I and II can be computed for different utilization ratios [35]. A summary of the optimization results is provided in Table 2. Notice first from this table that the flow ratio $r_{f,ST}$ in daytime operation is listed in every case. It can be seen that, when $\phi_{util} \le 1$, the same flexibility indices can be obtained with both configurations. This is because of the fact that, since the absorbed solar energy is consumed almost immediately and completely, the thermal storage tank in Configuration I is not needed at all, i.e., $r_{f,ST} = 0$. On the other hand, one can see that $r_{f,ST} = 1$ if $\phi_{util} > 1$, which implies that the thermal storage tank is fully utilized for storing the excess solar energy acquired during the daytime operation in Configuration I. Note that, although $r_{f,ST}$ is allowed to assume a real value between 0 and 1 in this situation, this optimal operating policy is adopted mainly to avoid violating the temperature upper bounds in Eqs. (2) and (12).

Note that the active constraint in each optimum solution, i.e., when $g_j = 0$ [18], is also given in Table 2. For $\phi_{util} < 1$, since the consumed energy may not be enough to meet the demand, the distillate tank is expected to be emptied at some instances. The optimization results of the corresponding two cases are analyzed below.

- Let us first consider Case 1 when $\phi_{util} = 0.79$. Note that $FI_t = 0$ in this case, i.e., no deviations from the nominal parameters are allowed for both configurations. This is due to the fact that the nominal absorption rate of solar energy is just enough to meet the nominal demand by maximizing the control variable $m_{f,MD}$ at all times.
- Let us next consider Case 2 when $\phi_{util} = 0.96$. Note that $FI_t = 1$ in this case, i.e., the expected deviations from the nominal parameters can be exactly accomodated in both configurations. To validate this

Table 1
Model parameters and variables.

Symbol	Definition	Value	Classification
$T_{f,SA_{out}}^{max}$	Maximum allowable outlet temperature of the solar absorber	100 °C	**d**
$M_{f,SA}$	Total mass of the operating fluid in the solar absorber	–	**d**
L_{SA}	Length of the absorber tube	–	**d**
A_{SA}	Exposed area in the solar absorber	–	**d**
Cp_f^L	Heat capacity of the operating fluid	4200 J/kg °C	**d**
$M_{f,ST}$	Total mass of the operating fluid in the thermal storage tank	10,000 kg	**d**
$m_{f,STL}$	Mass flow rate in the thermal loop	36,000 kg/h	**d**
$T_{f,HX,CL_{in}}$	Cold fluid inlet temperature of the heat exchanger	25 °C	**d**
A_{MD}	Membrane area of a standard AGMD module	10 m^2 [36]	**d**
n_{AGMD}	Total number of standard AGMD modules	–	**d**
STEC	Specific thermal energy consumption	14,000 kJ/kg [36]	**d**
$T_{f,HX,CL_{out}}^{max}$	Maximum cold fluid outlet temperature of the heat exchanger	90 °C	**d**
ρ_f^L	Distillate density	1000 kg/m^3	**d**
A_{DT}	Cross-sectional area of the distillate tank	0.35 m^2	**d**
$h_{DT,low}$	Lower bound of the liquid height in the distillate tank	0 m	**d**
$h_{DT,high}$	Upper bound of the liquid height in the distillate tank	2.14 m	**d**
ϕ_{util}	Energy utilization ratio	To be selected	**d**
$I(t)^{max}$	Maximum solar irradiation rate per unit area	1320 W/m^2	**d**
$m_{f,MD}^{max}$	Maximum mass flow rate in the membrane distillation loop	1237.5 kg/h	**d**
$T_{f,HX,CL_{in}}^{min}$	Minimum cold fluid inlet temperature of the heat exchanger	25 °C	**d**
$T_{f,SA_{in}}$	Inlet temperature of the solar absorber	–	**x**
$T_{f,SA_{out}}$	Outlet temperature of the solar absorber	–	**x**
$m_{f,SA}$	Mass flow rate of the operating fluid in the solar absorber	–	**x**
$T_{f,ST_{in}}$	Inlet temperature of the thermal storage tank	–	**x**
$T_{f,ST_{out}}$	Outlet temperature of the thermal storage tank	–	**x**
$m_{f,ST}$	Throughput of the thermal storage tank	–	**x**
$r_{f,ST}$	Flow ratio for the thermal storage tank	–	**x**
$m_{f,HX,HL}$	Mass flow rate of the hot fluid in the heat exchanger	–	**x**
$T_{f,HX,HL_{in}}$	Hot fluid inlet temperature of the heat exchanger	–	**x**
$T_{f,HX,HL_{out}}$	Hot fluid outlet temperature of the heat exchanger	–	**x**
$T_{f,HX,CLout}$	Cold fluid outlet temperature of the heat exchanger	–	**x**
h_{DT}	Liquid height in the distillate tank	–	**x**
$m_{f,DT_{in}}$	Inlet flow rate of the distillate tank	–	**x**
N_{mem}	Distillate flux through the AGMD membrane	–	**x**
$m_{f,MD}$	Mass flow rate in the membrane distillation loop	4500 kg/h (nominal)	**z**
I	Solar irradiation rate per unit area	–	**θ**
$m_{f,DT_{out}}$	Outlet flow rate of the distillate tank	—	**θ**

Table 2
Optimization results.

Configuration	Case no.	1	2	3	4	5	6	7
	ϕ_{util}	0.79	0.96	1	1.16	1.28	1.39	1.58
I	FI_t	0	1	1.24	1.65	1.65	1	0
	$r_{f,ST}$ (day)	0	0	0	1	1	1	1
	$g_j = 0$	$h_{DT,low}$	$h_{DT,low}$	$h_{DT,low}$	$h_{DT,low}$	$h_{DT,high}$	$h_{DT,high}$	$h_{DT,high}$
II	FI_t	0	1	1.24	1	0	Inf	Inf
	$r_{f,ST}$ (day)	0	0	0	0	0	N/A	N/A
	$g_j = 0$	$h_{DT,low}$	$h_{DT,low}$	$h_{DT,low}$	$T^{max}_{f,SA_{out}}$	$T^{max}_{f,SA_{out}}$	N/A	N/A

prediction, the worst-case scenario has been numerically simulated with Simulink® [39]. The Simulink program was coded according to Eqs. (1)–(15) and also the parameter values listed in Table 1. To facilitate the simulation run, three time profiles were adopted as inputs, i.e., (1) the lower limit of a solar irradiation profile in Fig. 4, (2) the upper limit of the water demand profile in Fig. 5, and (3) the control variable $m_{f,MD}(t)$ obtained by solving the temporal flexibility index model. The simulated temperature of the operating fluid at the exit of solar absorber (i.e., $T_{f,SA_{out}}$) and also that of sea water at the exit of heat exchanger (i.e., $T_{f,HX,CL_{out}}$) are both plotted in Fig. 6. It can be clearly observed that, at any time during a day, both temperatures are well below their respective upper bounds. The corresponding water level in distillate tank can also be found in Fig. 7. Note the tank is just emptied at the end of 24 h. This observation essentially confirms the optimization result of $FI_t = 1$ for both configurations. Thus, if the desired value of temporal flexibility index is one, Configuration II should be chosen since the equipment cost for a thermal storage facility can be saved.

In Case 3 when $\phi_{util} = 1$, notice that the optimization results are still the same for both configurations, i.e., $r_{f,ST} = 0$ in daytime operations and $FI_t = 1.24$. If the target value of temporal flexibility index is 1, then Configurations I and II in this case are both slightly overdesigned since $FI_t > 1$. However, if a higher operational flexibility is called for in design, then there is an incentive to consider additional cases in which the solar absorbers are larger, i.e., $\phi_{util} > 1$. The following are the corresponding case studies.

- In Case 4 ($\phi_{util} = 1.16$), Configuration I can be made more flexible ($FI_t = 1.65$) by operating the thermal storage tank, i.e., $r_{f,ST} = 1$. The corresponding worst-case scenario can be simulated and the time profiles of three critical variables, i.e., $T_{f,SA_{out}}$, $T_{f,HX,CL_{out}}$ and h_{DT}, can be found in Figs. 8 and 9. On the other hand, note that the temporal flexibility index of Configuration II equals one. This is because, since there is no thermal storage capacity, the exit temperature of the solar absorber ($T_{f,SA_{out}}$) reaches its upper limit at certain instance during the daytime operation which can occur when the solar irradiation is high. The corresponding system behavior (high solar irradiation and low water demand) can be characterized with Figs. 10 and 11.
- In Case 5 ($\phi_{util} = 1.28$), the temporal flexibility index of Configuration I can be raised to 1.65 and the active constraint is now associated with the upper bound of water level in distillate tank, i.e., $h_{DT} \le h_{DT,high}$. This is obviously due to the fact that the solar energy is introduced at a rate which is much faster than the consumption rate of thermal energy. On the other hand, note that $FI_t = 0$ for Configuration II. This drastic reduction of flexibility can also be attributed to the high intake rate of solar energy. Since there is no thermal storage tank, it is very difficult to keep the exit temperature of the solar absorber ($T_{f,SA_{out}}$) below 100 °C.
- In Case 6 ($\phi_{util} = 1.39$) and Case 7 ($\phi_{util} = 1.58$), the selected solar absorbers are larger than those used in the other cases. Since more water is produced in Configuration I while the size of the distillate tank remains the same in either Case 6 or 7, the resulting flexibility index becomes much lower than that achieved

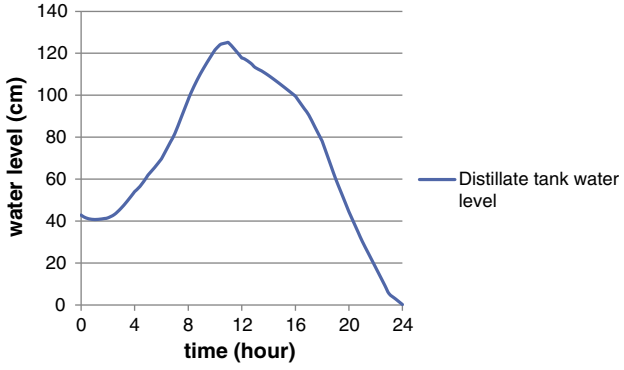

Fig. 7. The time profiles of h_{DT} for both configurations in the worst-case scenario ($\phi_{util} = 0.96$).

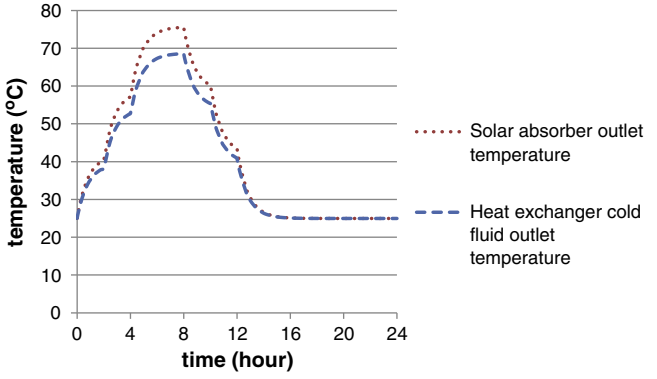

Fig. 6. The time profiles of $T_{f,SA_{out}}$ and $T_{f,HX,CL_{out}}$ for both configurations in the worst-case scenario ($\phi_{util} = 0.96$).

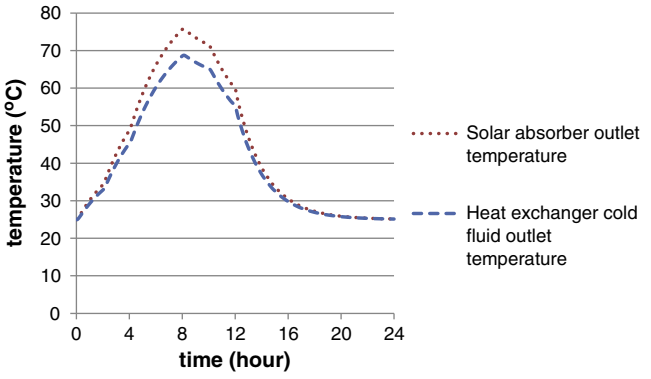

Fig. 8. The time profiles of $T_{f,SA_{out}}$ and $T_{f,HX,CL_{out}}$ for Configuration I in the worst-case scenario ($\phi_{util} = 1.16$).

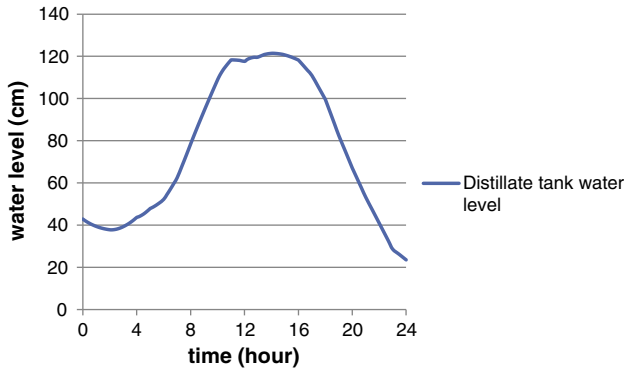

Fig. 9. The time profile of h_{DT} for Configuration I in the worst-case scenario ($\phi_{util} = 1.16$).

in Case 5. On the other hand, note that $FI_t = 0$ for Configuration II in Case 5. Thus, any further increase in the utilization ratio inevitably renders Configuration II infeasible.

If there is a need to make the SMDDS system even more flexible ($FI_t > 1.65$), one can deduce from Case 5 that this goal can be reached by relaxing the active constraint, i.e., by enlarging the thermal storage tank ($M_{f,ST} \geq 10{,}000$ kg) and also the distillate tank ($h_{DT,high} \geq 2.14$ m). Finally, it should be noted that the temporal flexibility may be further enhanced by introducing additional structural modifications, e.g., by operating more than one thermal storage tank in parallel. The merits of these new configurations can be easily assessed on the basis of the proposed temporal flexibility analysis.

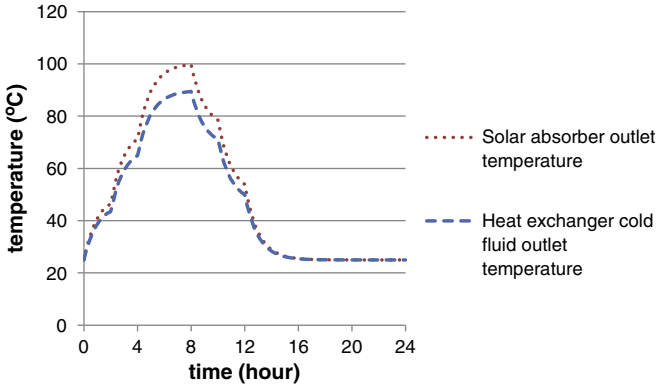

Fig. 10. The time profiles of $T_{f,SA_{out}}$ and $T_{f,HX.CL_{out}}$ for Configuration II in the worst-case scenario ($\phi_{util} = 1.16$).

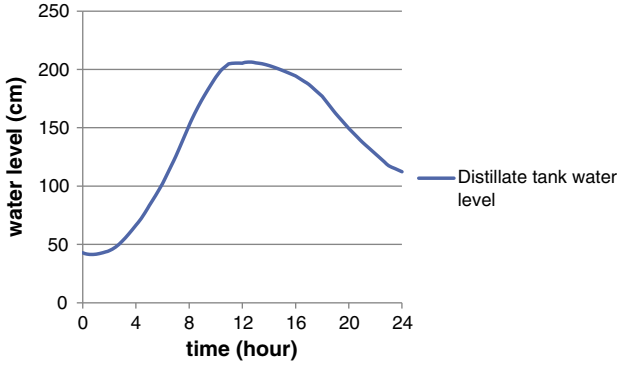

Fig. 11. The time profile of h_{DT} for Configuration II in the worst-case scenario ($\phi_{util} = 1.16$).

5. Conclusions

As mentioned previously, the ability of a system to maintain feasible operation despite unexpected disturbances is referred to as its *operational flexibility*. A systematic SMDDS design strategy is thus developed in this work on the basis of the temporal flexibility index. Given a system configuration, all units can be properly sized to achieve a target degree of flexibility. Given a fixed SMDDS design, additional enhancement measures can be identified according to the active constraints embedded in the optimum solution of the flexibility index model. These measures for further refinements include modifications in unit sizes and/or system structure. Finally, the optimization and simulation results obtained in case studies show that the proposed approach is convenient and effective for addressing various operational issues in SMDDS design.

Nomenclature

Acronyms

AGMD	Air gap membrane distillation
DAE	Differential-algebraic equation
FI	Flexibility index
MINLP	Mixed integer nonlinear programming
PTFE	Polytetrafluoroethylene
SMDDS	Solar-driven membrane distillation desalination system
STEC	Specific thermal energy consumption

Variables

$\mathbf{d}$	Vector of design variables
f	Equality constraints
g	Inequality constraints
h	Equality constraints, height
m	Mass flow rate
r	Ratio
t	Time
$\mathbf{x}$	Vector of state variables
$\mathbf{z}$	Vector of control variables
wdf	Water demand factor
A	Cross-sectional area
H	Operation horizon
I	Solar irradiation
L	Length
M	Total volumetric mass
N	Mass flux
T	Temperature
Cp	Heat capacity
FI	Flexibility index
STEC	Solar thermal energy conversion constant
$\mathbb{I}$	Set of equality constraints
$\mathbb{J}$	Set of inequality constraints

Greek letters

δ	Deviation due to uncertainties
Δ	Expected deviations
ρ	Liquid density
τ	Time
θ	Uncertain parameters
$\boldsymbol{\theta}$	Vector of uncertain parameters
Θ	Accumulated uncertainty parameters

Superscripts

$+$	Positive direction
$-$	Negative direction
0	Variable at $t = 0$
L	Liquid state

N	Nominal values
max	Maximum
min	Minimum

Subscripts

d	Dynamic
f	Fluid
i	Label of equality constraint
j	Label of inequality constraint
s	Steady state
t	Temporal
0	Variable at the beginning of interval 0
1	Variable at the end of interval 1
high	High limit
in	Inlet
low	Low limit
out	Outlet
util	Utilization ratio
mem	Membrane
BP	By-pass
CL	Cold liquid
DT	Distillate tank
HL	Hot liquid
HX	Heat exchanger
MD	Membrane distillation
SA	Solar absorber
ST	Storage tank
STL	Solar thermal loop

Acknowledgement

The authors wish to thank Prof. H. Chang and Prof. Y. H. Chen from the Department of Chemical and Materials Engineering, Tamkang University, Taiwan for their useful suggestions in constructing the system model for the SMDDS process. The authors also wish to thank Prof. W. Wu from the Department of Chemical Engineering, National Cheng Kung University, Taiwan for his useful insights for the household water demand assumption.

References

[1] C. Cabassud, D. Wirth, Membrane distillation for water desalination: how to choose an appropriate membrane? Desalination 157 (2003) 307–314.
[2] H. Ben Bacha, T. Dammak, A.A. Ben Abdalah, A.Y. Maalej, H. Ben Dhia, Desalination unit coupled with solar collectors and storage tank: modeling and simulation, Desalination 206 (2007) 341–352.
[3] V.A. Bui, L.T.T. Vu, M.H. Nguyen, Simulation and optimization of direct contact membrane distillation for energy efficiency, Desalination 259 (2010) 29–37.
[4] J. Koschikowski, M. Wieghaus, M. Rommel, Solar thermal-driven desalination plants based on membrane distillation, Desalination 156 (2003) 295–304.
[5] G.W. Meindersma, C.M. Guijt, A.B. de Haan, Desalination and water recycling by air gap membrane distillation, Desalination 187 (2006) 291–301.
[6] H. Chang, G.B. Wang, Y.H. Chen, C.C. Li, C.L. Chang, Modeling and optimization of a solar driven membrane distillation desalination system, Renew. Energy 35 (2010) 2714–2722.
[7] H. Chang, S.G. Lyu, C.M. Tsai, Y.H. Chen, T.W. Cheng, Y.H. Chou, Experimental and simulation study of a solar thermal driven membrane distillation desalination process, Desalination 286 (2012) 400–411.
[8] J.B. Gálvez, L. García-Rodríguez, I. Martín-Mateos, Seawater desalination by an innovative solar-powered membrane distillation system: the MEDESOL project, Desalination 246 (2009) 567–576.
[9] E. Guillen-Burrieza, J. Blanco, G. Zaragoza, D.C. Alarcon, P. Palenzuela, M. Ibarra, W. Gernjak, Experimental analysis of an air gap membrane distillation solar desalination pilot system, J. Membr. Sci. 379 (2011) 386–396.
[10] A. Malcom, J. Polan, L. Zhang, B.A. Ogunnaike, A.A. Linninger, Integrating systems design and control using dynamic flexibility analysis, AICHE J. 53 (2007) 2048–2061.
[11] F.V. Lima, C. Georgakis, Design of output constraints for model-based non-square controllers using interval operability, J. Process. Control. 18 (2008) 610–620.
[12] F.V. Lima, C. Georgakis, J.F. Smith, P.D. Schnelle, D.R. Vinson, Operability-based determination of feasible control constraints for several high-dimensional nonsquare industrial processes, AICHE J. 56 (2009) 1249–1261.
[13] F.V. Lima, Z. Jia, M. Ierapetritou, C. Georgakis, Similarities and differences between the concepts of operability and flexibility: the steady-state case, AICHE J. 56 (2010) 702–716.
[14] R.E. Swaney, I.E. Grossmann, An index for operational flexibility in chemical process design part I: formulation and theory, AICHE J. 31 (1985) 621–630.
[15] R.E. Swaney, I.E. Grossmann, An index for operational flexibility in chemical process design part II: computational algorithms, AICHE J. 31 (1985) 631–641.
[16] I.E. Grossmann, K.P. Halemane, Decomposition strategy for designing flexible chemical plants, AICHE J. 28 (1982) 686–694.
[17] K.P. Halemane, I.E. Grossmann, Optimal process design under uncertainty, AICHE J. 29 (1983) 425–433.
[18] I.E. Grossmann, C.A. Floudas, Active constraint strategy for flexibility analysis in chemical process, Comput. Chem. Eng. 11 (1987) 675–693.
[19] D.K. Varvarezos, I.E. Grossmann, L.T. Biegler, A sensitivity based approach for flexibility analysis and design of linear process systems, Comput. Chem. Eng. 19 (1995) 1301–1316.
[20] V. Bansal, J.D. Perkins, E.N. Pistikopoulos, Flexibility analysis and design of linear systems by parametric programming, AICHE J. 46 (2000) 335–354.
[21] G.M. Ostrovski, L.E.K. Achenie, Y.P. Wang, Y.M. Volin, A new algorithm for computing process flexibility, Ind. Eng. Chem. Res. 39 (2001) 2368–2377.
[22] C.A. Floudas, Z.H. Gunus, M.G. Ierapetritou, Global optimization in design under uncertainty: feasibility test and flexibility index problems, Ind. Eng. Chem. Res. 40 (2001) 4267–4282.
[23] G.M. Ostrovski, Y.M. Volin, Flexibility analysis of chemical process: selected global optimization sub-problems, Optim. Eng. 3 (2002) 31–52.
[24] V. Bansal, J.D. Perkins, E.N. Pistikopoulos, Flexibility analysis and design using a parametric programming framework, AICHE J. 48 (2002) 2851–2867.
[25] Y.M. Volin, G.M. Ostrovski, Flexibility analysis of complex technical systems under uncertainty, Autom. Remote. Control. 63 (2002) 1123–1136.
[26] V.S.K. Adi, C.T. Chang, Two-tier search strategy to identify nominal operating conditions for maximum flexibility, Ind. Eng. Chem. Res. 50 (2011) 10707–10716.
[27] C.T. Chang, B.H. Li, C.W. Liou, Development of a generalized mixed integer nonlinear programming model for assessing and improving the operational flexibility of water network designs, Ind. Eng. Chem. Res. 48 (2009) 3496–3504.
[28] E. Riyanto, C.T. Chang, A heuristic revamp strategy to improve operational flexibility of water networks based on active constraints, Chem. Eng. Sci. 65 (2010) 2758–2770.
[29] E.N. Pistikopoulos, I.E. Grossmann, Optimal retrofit design for improving process flexibility in linear systems, Comput. Chem. Eng. 12 (1988) 719–731.
[30] E.N. Pistikopoulos, I.E. Grossmann, Evaluation and redesign for improving flexibility in linear systems with infeasible nominal conditions, Comput. Chem. Eng. 12 (1988) 841–843.
[31] E.N. Pistikopoulos, I.E. Grossmann, Optimal retrofit design for improving process flexibility in nonlinear systems — I: fixed degree of flexibility, Comput. Chem. Eng. 13 (1989) 1003–1016.
[32] E.N. Pistikopoulos, I.E. Grossmann, Optimal retrofit design for improving process flexibility in nonlinear systems — II: optimal level of flexibility, Comput. Chem. Eng. 13 (1989) 1087–1096.
[33] N.C. Petracci, P.M. Hoch, A.M. Cliche, Flexibility analysis of an ethylene plant, Comput. Chem. Eng. 20 (1996) S443–S448.
[34] V.D. Dimitriadis, E.N. Pistikopoulos, Flexibility analysis of dynamic systems, Ind. Eng. Chem. Res. 34 (1995) 4451–4462.
[35] V.S.K. Adi, C.T. Chang, Dynamic flexibility analysis with differential quadratures, Comp. Aid. Chem. Eng. 31 (2012) 260–264.
[36] F. Banat, N. Jwaied, M. Rommel, J. Koschikowski, M. Wieghaus, Performance evaluation of the "large SMADES" autonomous desalination solar-driven membrane distillation plant in Aqaba, Jordan, Desalination 217 (2007) 17–28.
[37] G. Burgess, K. Lovegrove, Solar thermal powered desalination: membrane versus distillation technologies, http://solar-thermal.anu.edu.au/files/2010/02/DesalANZSES05.pdf, (Accessed April 2013).
[38] L.T. Biegler, I.E. Grossmann, A.W. Westerberg, Systematic methods of chemical process design, Prentice-Hall, Englewood Cliffs, New Jersey, 2007, pp. 690–714.
[39] The Mathworks, Inc., Simulink® getting started guide, http://www.mathworks.com/help/pdf_doc/simulink/sl_gs.pdf, (Accessed April 2013).